# Cellular structures for use in composite panels with a mass distribution gradient produced by additive manufacturing

**Bernardo Garrido Marques da Silva**

garrido.bernardo95@gmail.com

Instituto Superior Técnico, Universidade de Lisboa, Portugal

**January 2021**

## Abstract

The present work aims to evaluate the flexural properties of functionally graded cellular materials (FGCM) and compare them to more traditional homogeneous honeycomb structures, used as sandwich panels.

For that purpose, three cellular configurations were analyzed, namely Hexagonal, Lotus and Hexagonal with Plateau borders, as initially proposed by Ronan et al. [1]. Graded structures with different density gradients (G parameter) were also studied. The effect of the angle of rotation was also evaluated. The materials used for the structures were PLA (Polylactic Acid) and an aluminum alloy. The structures were designed using CAD software Solidworks and were manufactured by FFF (Fused Filament Fabrication). The flexural properties of the FGCM were analyzed by performing three-point bending tests, both experimentally and also by means of FEA (Finite Element Analysis).

Results show that FGCM structures perform better than regular honeycomb structures, both in strength and stiffness. Lotus structures performed better than regular honeycomb structures for 0-degree rotation geometries, whereas Plateau structures show a better performance with a 90-degree rotation of the geometry. It was also shown that the higher the G-parameter value, the better the mechanical performance of the structures is, both in initial stiffness and absorbed energy.

Consequently, FGCM structures have shown to be an alternative to the traditional honeycomb structures used in sandwich composite panels in a varied range of applications, where low weight and high stiffness of structures are requirements.

**Key-words:** FGCM, G parameter, FEA, FFF, SLM, Three-point bending test

# Introduction

In recent years, some new types of structures have been studied in pursuit of better structural elements. One of the major goals of structural design is to achieve load-carrying structures as light as possible, with high stiffness and strength.

Functionally graded cellular materials (FGCM) are materials where its characteristics change with its composition and structure. FGCM are a blend of functionally graded materials with cellular materials [2].

FGCM represents a new class of composites that consists of graded pattern of material composition and/or microstructures. They are a new emerging class of advanced materials, very attractive for an extensive range of engineering applications because they enable the design of different functional performances within a part. These materials have captured the interest of the scientific community, resulting in several investigations and technology applications [3].

Cellular materials, such as open or closed foams, honeycombs, and metal hollow spheres, are a new class of ultra-light multi-functional materials that can withstand large deformation at a nearly constant Plateau stress [4]. These materials can absorb a large amount of energy before collapsing to a more stable configuration. They can be attached as sacrificial layers to protect structures, machines, and infrastructures against dynamic events. The cladding is expected to sustain damage during impact or blast loading, thereby mitigating the extent of destruction of the main structures. The properties of cellular materials assist in dispersing the energy and impulse transmitted into the structure and consequently protect objects located behind them [5].

The grading can be made by several methods. It can occur by changing the distribution of the core size, the thickness of the core walls, the density or even the properties of the material [6].

Some authors have reported that many improved properties were imparted by graded cellular structures which could not be achieved by the uniform cellular structures [7].

These structures have a wide range of

application in the aerospace and automotive industries that require low weight, high bending strength, and high energy absorption and low heat absorption [5].
The main goal of this paper is to study the mechanical properties of functional graded cellular material with three different core designs, namely, Hexagonal, Plateau and Lotus as well as two different orientation angles. The aim is to search for designs with better mechanical properties, maintaining the lightness which is characteristic of honeycomb structures.

# Materials and methods

For the purposes of this research, three distinct cellular structures were designed, more specifically Hexagonal, Lotus and Plateau (Figure 1), with the objective of analyzing which of these designs performed the best in different aspects by performing three-point bending tests.


*Figure 1 - A- Hexagonal core, B- Lotus core and C- Plateau core.*

The FGCM have a density gradient, measured by the G parameter, which characterizes the density gradient.
In total, twenty-three structures were created using Solidworks 2018 student edition software, organized by sets of five (one Hexagonal, one Lotus, one Plateau, one Upperbound and one Lowerbound). The Lower and Upperbound are respectively, the regular honeycomb structures with the largest and smallest core size. They are included in order to compare the FGCM structures with standard honeycombs. They act as control for the other structures. The nomenclature is set as the core design followed by the smallest and biggest wall thickness values.
Numerical simulations using finite element method (FEM) software Siemens NX 11 were performed for all twenty-three cases.
The set of structures have different G parameter and consequently different relative density values. From all structures, only five were chosen to be printed and to perform experimental tests with 0-degree rotation angle.
The dimensions of the parts are: 163.8x54x22 $mm^3$.

## Material

The materials used in this paper, both in simulations and in the printed structures were Polylactic Acid (PLA) and Aluminum-A for numerical simulations only. Structures were printed with PLA. The PLA was selected since it is one of the most used materials in FFF manufacturing. It is a biodegradable (degrades into innocuous lactic acid) thermoplastic polymer (aliphatic polyester) derived from renewable resources such as cornstarch or cereals [8]. It is one of the most popular bio plastics used, and it is very common in FFF additive manufacturing. Known for its good mechanical properties, such as its high modulus and high strength, this thermoplastic is used in a wide set of applications from food packaging and plastic cups to medical implants. Since its properties can change from case to case, differing because of manufacturing processes and specifications, the properties used in the present project are the following, as presented in Table 1 in accordance with the study conducted by Fernandes [9] in PLA compact specimens under linear tensile loading. The tables 1 and 2 present the properties of the PLA and Aluminum-A respectively:

*Table 1 - PLA properties.*

| **Density (g/cm$^3$)** | **1.252** |
|---|---|
| **Young's Modulus (MPa)** | 1750 |
| **Poisson's ratio** | 0.36 |
| **Tensile strength (MPa)** | 20 |
| **Elongation at break (%)** | 7 |

*Table 2 - Aluminum-A properties.*

| **Density (g/cm$^3$)** | **2.680** |
|---|---|
| **Young's Modulus (GPa)** | 59 |
| **Poisson's ratio** | 0.33 |
| **Tensile strength (MPa)** | 211 |
| **Elongation at break (%)** | 8 |

## Defining the G parameter

A very important parameter when analyzing functionally graded cellular structures is the one designated by G parameter, developed in the present work, in which G stands for gradient. The main purpose of this parameter is to quantify the density gradient in a FGCM structure. With this parameter, one can compare different structures with different density gradients. This parameter is computed using different measurements in the FGCM structure and it is illustrated in Figures 2 and 3.

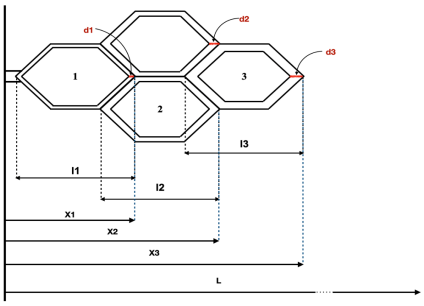


*Figure 2 - Schematic of variables used to define the G parameter.*

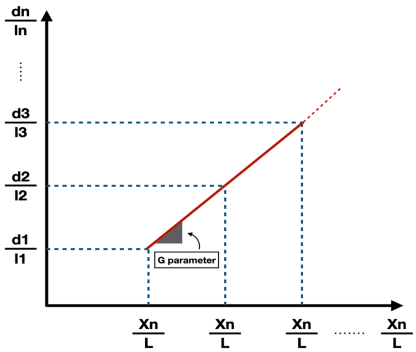


*Figure 3 - G parameter: seen as a slope.*

After obtaining the values for the different measurements, then a plot is made and the slope of the curve is the value of the G parameter. The larger the G parameter value, the higher the density gradient present in the structure.

## Finite element modeling

All the twenty-three structures were made in CAD software Solidworks 2018 Student Edition and after that were imported to FE software Siemens NX 18 version 1851 as .SLDPRT files. For the analysis process, for all structures, the software needs three types of files: part, fem and sim. After the sim file is created, a solver was used [10].

The part file is the starting point for each of the analyses performed. The model used can be created in the Siemens NX software or can be imported from different CAD software, which was the case. After importing the model, since the structures have two symmetric planes (coincident with half-length and half-width), created using *Datum Plane* command, and then using the *Split Body* command, the model becomes divided in four symmetrical pieces. Next, using *Hide* command only a quarter of the complete model was selected to be showed.

The .fem file is critical in achieving a good finite element analysis. It is arguably the most important file of the three. It is where the mesh is created and the materials are assigned to the different parts of the model. The mesh size used, after a mesh refinement convergence test was performed, was 0.25 mm in the contact regions and 0.5 mm in the rest.

The .sim file is the last part of the preparation for the analysis before running the solver. In this file, the constraints are defined and regions for the contacts are created.

Once the .sim file is completed with the constraints, a solver must be run to get results. The most important part is to define the type of solution to use according to the analysis wanted.. For all the tests, for the structural analyses, a linear static solution was used – *SOL 101 Linear Statics – Global Constrains*.

Finally, the convergence criterion used was defined as less than 5% changes in the von Mises stress values and then using prior to the lastmesh, so as to reduce the computational processing time and memory.

The parameters analyzed were the maximum nodal von Mises stress, the local von Mises nodal stress and the average von Mises stress (Figure 4, 5 and 6).

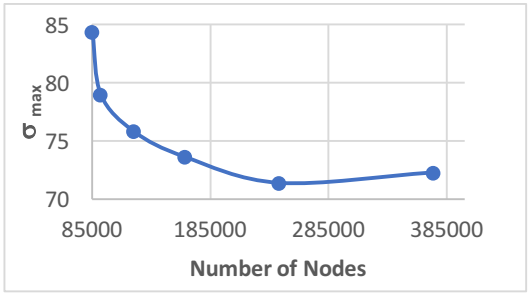


*Figure 4 - Maximum nodal von Mises stress vs number of nodes.*

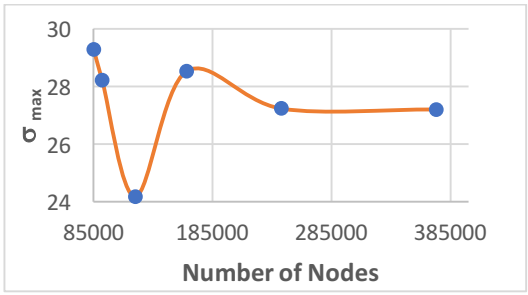


*Figure 5 - Local von Mises nodal stress vs number of nodes.*

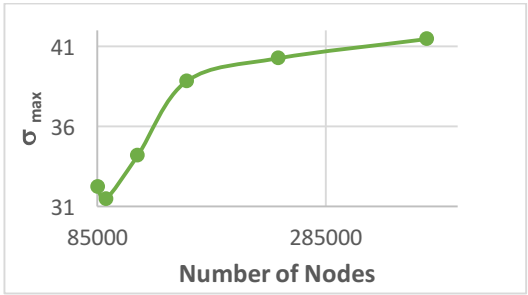


*Figure 6 - Average von Mises stress vs number of nodes.*

The smaller the mesh element sizes, the better

recreation of the real behavior of the structure. All the convergence tests started with element size being: 0.6 mm in the contact regions and 1 mm in the rest of the geometry. The convergence test was conducted using the thinner structure, being the one where the variation would be larger. The sizes utilized, once more, were 0.25 mm for the contact region and 0.5 mm for the rest of the geometry.

## Manufacturing

As mentioned before, all specimens were created in SolidWorks 2018 Student Edition *software*, and then were converted to stereolithographic files (.STL). Once the files were converted, they were imported to CURA software and then sent to the respective machines.
The PLA specimens were manufactured through the FFF method. It was used a Ultimaker 3 printer where some parameters need to be tuned. The most important parameters are the following: infill, layer thickness and temperatures of both the PLA filament and the printing bed. All the specimens were manufactured by an extruder with print core AA0.4 and 100% infill with closed chamber. After a few tune-ups, the parameters used were determined, as presented in Table 3.

*Table 3 - Printing parameters used.*

| Parameter | Value |
|---|---|
| Infill Speed | 90 (mm/s) |
| Outer Wall Speed | 50 (mm/s) |
| Travel Speed | 250 (mm/s) |
| Initial Layer Speed | 26 (mm/s) |
| Extrusion Temperature | 205 ºC |
| Built Plate Temperature | 70 ºC |
| Infill Overlap | 10 % |

The dimensions of the AM (Additive Manufacturing) structures have a small variation when compared to the intended dimensions (CAD dimensions). The height has 21 mm in the AM structure instead of 20 mm. It represents a dimensional error of 5 %. This error is negligible when analyzing both in length and in width.
The Aluminum-A specimens were intended to be manufactured through SLM method. The AlSi7Mg0.6 aluminum powder was selected to be used. Despite been chosen the material and printer, due to pandemic problems, these Aluminum-A structures were not able to be printed.

## Experimental 3PB test

The PLA specimens were subjected to the three-point bending test. The tests were made in accordance with norm ASTMC393-00 – Standard Test Method for Flexural Properties of Sandwich Constructions [11]. Figure 8 presents the experimental three-point bending test, in which the support span has a value of 150 mm for all experiments performed.
The equipment used to perform these tests was the Instron 3369 which is a dual column tabletop testing system and has a load cell of 50 kN. During all tests, the cross-head speed for the upper roller was defined to be 2.5 mm/min. Also during the experiments, the *Bluehill* software was used in order to obtain load-displacement curves.

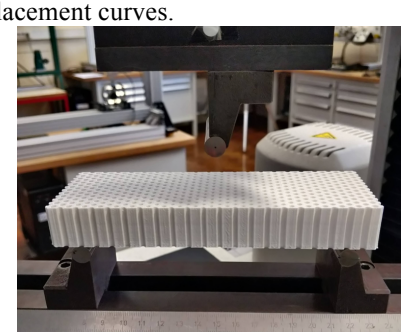

*Figure 7 -Experimental set-up for 3PB test.*

The procedures were as follows. First, once the machine is ready for the input of specimen parameters, these are given to the software. Despite the dimensions selected while designing the different structures, the dimensions after AM are slightly different in depth from the ones specified in CAD modeling (21 mm instead of 20 mm). The results are generated to several excel files where the information is presented as raw specimen data and flexural results.

# Results and discussion

In this section, some comments about the comparison of mechanical behaviour both from numerical simulations and also from experiments, in the case of Additive Manufactured PLA structures subjected to the 3-PB tests. For the Aluminum-A structures, only numerical results were obtained. For all numerical results, the results presented are for a quarter of the geometry.

## PLA numerical results

The following results show the values of relative density and G parameters, and the values of von Mises stress, the slope of the linear region load-displacement curve (stiffness), and the absorbed energy. The parameters von Mises stress, slope of the linear region and the absorbed energy were

normalized with respect to the relative density. The data is presented in different tables, for each value of the G parameter and by angle of rotation.

All the parameters were obtained using the Siemens NX *software,* where the respective *output requests* were selected and analyzed. The first three tables present the values for 0-degree angle of rotation. Each table represents a set of structures with the same G parameter (Hexagonal core, Plateau core and Lotus core structures) as well as the respective Lowerbound and Upperbound. The Lowerbound and Upperbound structures, are both homogeneous Hexagonal core structures (no density gradient), where the Lowerbound has the smallest wall thickness and the Upperbound has the bigger wall thickness. These two structures are used as testing, providing the upper and Lowerbound values for traditional honeycomb structures.

Table 4,5 and 6 presents the respective relative density of each structure (0-degree angle of rotation), the G parameter and the values of the maximum von Mises stress, initial stiffness, absorbed energy corrected with relative density. Figure 7 presents the results for the 90-degree angle of rotation structures.

*Table 4 - Values of relative density, G parameter and values of stress, initial stiffness, absorbed energy corrected with relative density for different structures* (G =0.212).

| Geometry | $\bar{\rho}$ | $\bar{\sigma}_y/\bar{\rho}$ (MPa) | K/$\bar{\rho}$ (N/mm) | $E_a/\bar{\rho}$ (N.mm) | G parameter |
|---|---|---|---|---|---|
| **Lowerbound d0.25** | 0.210 | 339.11 | 38.59 | 109.15 | - |
| **Hexagonal d0.25-1.25** | 0.552 | 154.57 | 271.09 | 315.56 | 0.212 |
| **Plateau d0.25-1.25** | 0.554 | 151.10 | 277.85 | 379.41 | 0.212 |
| **Lotus d0.25-1.25** | 0.589 | 143.77 | 292.25 | 460.27 | 0.212 |
| **Upperbound d1.25** | 0.803 | 133.83 | 258.21 | 323.19 | - |

*Table 5 - values of relative density, G parameter and values of stress, initial stiffness, absorbed energy corrected with relative density for different structures (G =0.105).*

| Geometry | $\bar{\rho}$ | $\bar{\sigma}_y/\bar{\rho}$ (MPa) | K/$\bar{\rho}$ (N/mm) | $E_a/\bar{\rho}$ (N.mm) | G parameter |
|---|---|---|---|---|---|
| **Lowerbound d0.25** | 0.210 | 339.11 | 38.60 | 109.15 | - |
| **Hexagonal d0.25-0.75** | 0.399 | 191.38 | 167.81 | 310.08 | 0.105 |
| **Plateau d0.25-0.75** | 0.401 | 177.70 | 182.01 | 377.60 | 0.105 |
| **Lotus d0.25-0.75** | 0.455 | 175.45 | **236.47** | **396.76** | 0.105 |

*Table 6 - values of relative density, G parameter and values of stress, initial stiffness, absorbed energy corrected with relative density for different structures (G =0.091).*

| Geometry | $\bar{\rho}$ | $\bar{\sigma}_y/\bar{\rho}$ (MPa) | K/$\bar{\rho}$ (N/mm) | $E_a/\bar{\rho}$ (N.mm) | G parameter |
|---|---|---|---|---|---|
| **Lowerbound d 0.80** | 0.585 | 137.52 | 179.27 | 285.88 | - |
| **Hexagonal d0.80-1.20** | 0.684 | 151.92 | 248.77 | 303.08 | 0.091 |
| **Plateau d0.80-1.20** | 0.685 | 155.80 | 254.19 | 299.61 | 0.091 |
| **Lotus d0.80-1.20** | 0.713 | 129.29 | **271.98** | **412.42** | 0.091 |
| **Upperbound d1.20** | 0.782 | 147.58 | 250.41 | 303.61 | - |

*Table 7 - Values of relative density, G parameter and values of stress, initial stiffness, Absorbed Energy corrected with relative density for different structures (G =0.677).*

| Geometry | $\bar{\rho}$ | $\bar{\sigma}_y/\bar{\rho}$ (MPa) | K/$\bar{\rho}$ (N/mm) | $E_a/\bar{\rho}$ (N.mm) | G parameter |
|---|---|---|---|---|---|
| **Lowerbound d0.74** | 0.431 | 140.109 | 127.226 | 298.426 | - |
| **Hexagonal d0.74-d1.48** | 0.678 | 148.486 | 306.107 | 347.481 | 0.677 |
| **Plateau d0.74-d1.48** | 0.679 | 152.503 | 275.090 | 408.438 | 0.677 |
| **Lotus d0.74-d1.48** | 0.687 | 126.876 | 287.099 | 403.438 | 0.677 |
| **Upperbound d1.48** | 0.866 | 124.838 | 263.046 | 286.097 | - |

For a G parameter of 0.212 it is possible to verify that the core structure design with highest $E_a$ and highest K is the Lotus. Lotus, is followed by Plateau and then Hexagonal as the structures that attain the highest values of specific K and Ea, although this tendency is more clearly marked for the steeper gradients. Concerning the von Mises stress, the situation is less well defined, but the Lowerbound structures seem to have a small advantage.

For G parameter of 0.105, the core structure design with highest values, for both $E_a$ and K, is Lotus. Then, both for K and $E_a$, the second highest results were achieved by the Plateau structure. The third were obtained with the Hexagonal structure. The structure with highest von Mises stress is the Lowerbound structure.

For G parameter of 0.091, the core structure design with better performance, i.e. highest values for $E_a$ and K, is the Lotus. The second highest K was obtained with the Plateau structure and the second highest value of $E_a$ was obtained with the Upperbound structure. The third K was for the Upperbound structure and the third of $E_a$ was for the Hexagonal structure.

The core design with highest value for von Mises stress is the Plateau.

For 90-degree angle of rotation structures, Table 7 presents the numerical results.

For the 90-degree structures (Table 7), the numerical results show that the best results for von Mises stress were obtained by Plateau structure, being the second-best results achieved with Hexagonal and then followed by the Lowerbound structure. For K, the highest value was obtained by the Hexagonal structure, followed by the Lotus and then the Plateau structure. When analyzing the $E_a$, it is observable that the structure that performed best was the Plateau structure, followed by the Lotus and then, the Hexagonal structure.

For the structures with 0-degree angle of rotation, Figure 8,9 and 10 sums up the values, and allows a better comparison between them. Figure 8, compares the values of **σ** between the different structures and sums up the information from the tables above. Figure 9, compares the values of K. Figure 10, compares the values of $E_a$. In Figure 9, there is no superlative core design, although the Lotus core design presented always the lower values. The Figure 9 compares the K for the different core designs for the different G parameters. In this case, the best performer was the Lotus structure and the worst results were obtained with the Hexagonal.

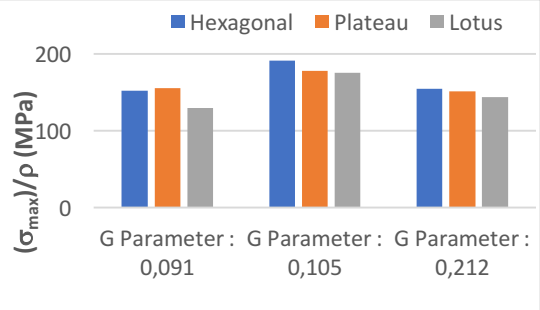


*Figure 8 – Graphical comparison of the von Mises stress normalized by relative density between Hexagonal, Plateau and Lotus cores.*

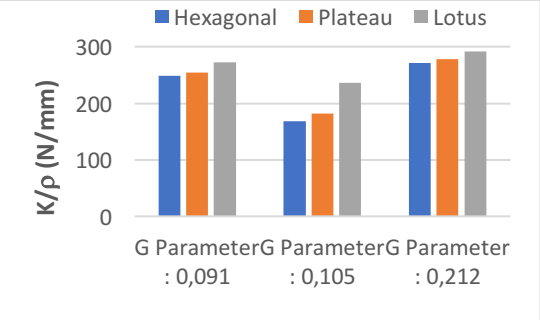


*Figure 9 - Graphical comparison of the initial stiffness normalized by relative density between Hexagonal, Plateau and Lotus cores.*

The last plot (Figure 10) compares the absorbed energy for each structure. It is clear, by observing, that the best output was obtained with Lotus and the worst was with Hexagonal.

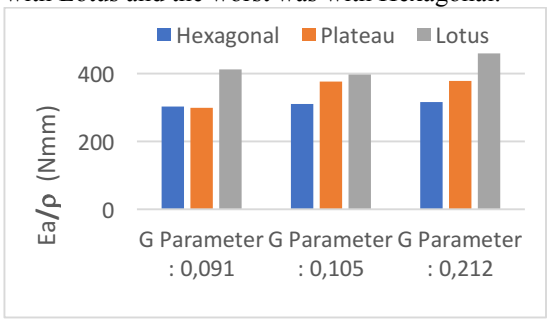


*Figure 10 Graphical comparison of the absorbed energy normalized by relative density between, Hexagonal, Plateau and Lotus cores.*

The explanation offered for the higher von Mises values observed with the Hexagonal structure lies in the presence of sharp edges acting as stress concentrators. On the other hand, the small radius of the Plateau design also induces some stress concentration. From this standpoint, the most advantageous structure is the Lotus.

There is no clear evidence, by analyzing the plots shown before, that there is a direct correlation between the G parameter and the increase of the performance. There is although, a very clear advantage of the FGCM structures performance compared to the structures without G parameter, being those the regular honeycomb structures.

Figure 11, which are prints from *Siemens NX,* show the numerical results for the 3PB loading.

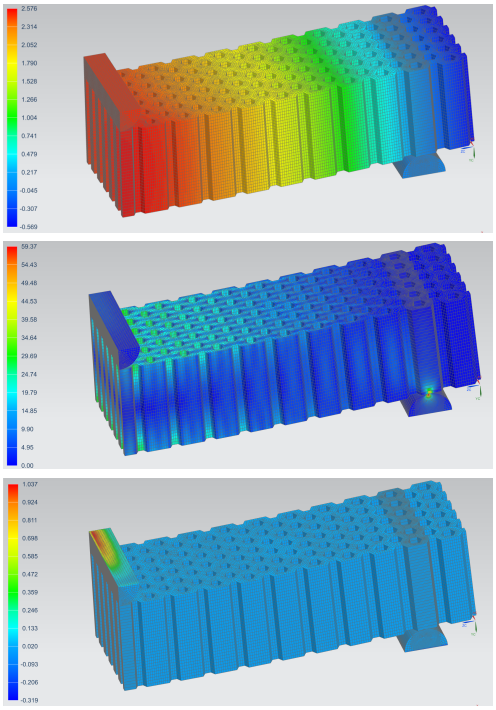

*Figure 11 - FEA of a Hexagonal structure (G=0.091) under 3PB loading, one quarter of the geometry showed: a) displacement of the model and rollers, b) von Mises stress in the skins and c) rollers reaction force in z-axis.*

It features the displacement of the part and the roller, the von Mises stress and the rollers reaction force in z-axis. Only a quarter of the geometry was simulated because of the symmetry conditions.

## Aluminum-A numerical results

For the Aluminum-A structures (Table 8), the numerical results show that the best results for K were achieved by Lotus structures, followed by Plateau and then Hexagonal. For the absorbed energy, the higher values were achieved by Plateau structures, followed by Lotus and then Hexagonal. In both parameters, the structures which have a G parameter performed better than those which do not have. The structure that presented a highest von Mises stress was the Lowerbound, followed by the Plateau and then followed by the Hexagonal.

*Table 8 - Values of relative density, G parameter and values of stress, initial stiffness, Absorbed Energy corrected with relative density for different structures (G =0.080).*

| Geometry | $\bar{\rho}$ | $\bar{\sigma}_y/\bar{\rho}$ (MPa) | K/$\bar{\rho}$ (N/mm) | $E_a/\bar{\rho}$ (N.mm) | G parameter |
|---|---|---|---|---|---|
| **Lowerbound d 0.82** | 0.579 | 11632.33 | 22146.22 | 31799.84 | - |
| **Hexagonal d0.82-1.17** | 0.678 | 9745.82 | 30077.33 | 33345.57 | 0.080 |
| **Plateau d0.82-1.17** | 0.679 | 11346.95 | 30519.23 | 43770.98 | 0.080 |
| **Lotus d0.82-1.17** | 0.708 | 8820.90 | 31888.51 | 39450.69 | 0.080 |
| **Upperbound d1.17** | 0.768 | 9451.84 | 29670.27 | 32334.69 | - |

## PLA experimental results

The experimental part was executed with only one G parameter, 0.091, as the specimens with better dimensions for AM were selected.

After accomplishing the experimental tests, the raw data from *Bluehill* software was used and the results are shown in Table 9. The results will be presented until 2.5 mm of vertical displacement to compare with the numerical results. The entire Load vs Displacement curve will be analyzed as well. All geometries had three samples each.

*Table 9 - Average and standard deviation values of load until breaking, initial stiffness and absorbed energy.*

| Structure | $\bar{\rho}$ | Load/$\bar{\rho}$ (kN) | ± | K/$\bar{\rho}$ (N/mm) | ± | Ea/$\bar{\rho}$ (N.mm) | ± |
|---|---|---|---|---|---|---|---|
| **Lowerbound** | 0.585 | 1.83 | 0.49 | 806.22 | 111.59 | 2112.53 | 3.43 |
| **Hexagonal** | 0.684 | 3.47 | 0.24 | 1544.64 | 51.18 | 4005.71 | 2.21 |
| **Plateau** | 0.685 | 3.18 | 0.70 | 1375.80 | 217.53 | 3751.66 | 0.08 |
| **Lotus** | 0.713 | 3.14 | 0.17 | 1375.61 | 23.55 | 3691.85 | 0.62 |
| **Upperbound** | 0.782 | 2.50 | 0.27 | 1098.04 | 18.96 | 2927.55 | 5.41 |

In the experimental tests, the functional graded cellular materials (Hexagonal, Plateau and Lotus) had a better performance. It is visible that any of the FGCM structures performed better than the other homogeneous cellular structures (Lowerbound and Upperbound). The load needed for a displacement of 2.5 mm was higher for the Hexagonal structure, then for the Plateau structure and then for the Lotus structure. The lower value, as expected was achieved by the Lowerbound structure. The Upperbound structure, despite being the geometric upper bound specimen, did not performed as so.

The highest value for K was obtained with the Hexagonal configuration, the second highest value was performed by the Plateau structure. The third highest value, being almost the same value as the Plateau , was obtained with the Lotus structure. Both homogeneous structures did not perform as good as the functional graded cellular structures in this case.

The highest $E_a$ value was obtained by the Hexagonal configuration, followed by the Plateau configuration and then by the Lotus . Both homogeneous structures did not perform as well as the functional graded cellular structures. Figure 12 presents the load-displacement curves until breaking for the different configurations.

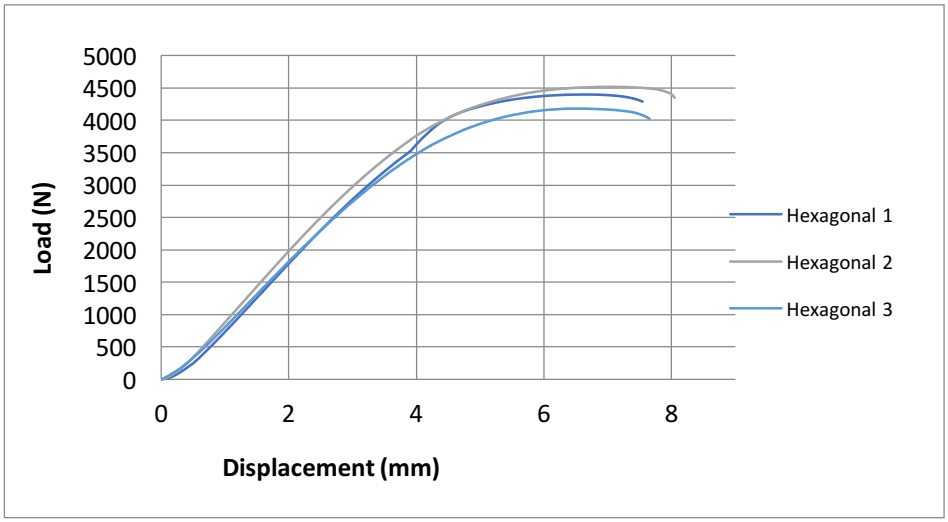


*Figure 12 - Load vs Displacement experimental results graphic of Hexagonal samples (G=0.091).*

## Failure observations

Failure surfaces were observed for all PLA samples. In all photographs (Figure 13) two lines are exhibited : in red the failure behavior and in blue the mid-section of each specimen. Only for Lowerbound and Upperbound samples, the red line and blue line correspond for a same cell thickness. In all others, the blue line corresponds to the mid-section of the specimens and consequently has a thicker cell than a red line, which is not coincident, because the core wall size increases from the edges to the middle of the structures.

The deviation relative to the mid-section of the sample can be caused by the indenter not being completely parallel to X axis, or by other issues. All three Hexagonal samples presented similar failure results. The failure is well visible, which happens inside the core. The failure mode for the three Plateau samples is very similar to the failure mode in the Hexagonal specimens. The failure is well visible inside the core. The propagation of the failure does not happen through the mid-section of the structure. This can be related, also to the diameter of the upper roller that does not contact on the surface as only one line, but in a certain area.

The Lotus samples presented all the same failure behavior. The failure occurred around the Lotus core and far from the mid-section of the structure.

The Upperbound samples performed as expected. The failure occurred inside the core and along the mid-section of the structure. All three samples presented the same failure results.

The Lowerbound samples all performed similarly. The Lowerbound structures were the ones with higher displacement. Because of that, and since the structures are subjected to both bending and stretching in addition to other effects as shearing, torsion and nodal interactions, these effects are well visible in the Lowerbound case. The failure occurred inside the core and near the mid-section of the specimens.

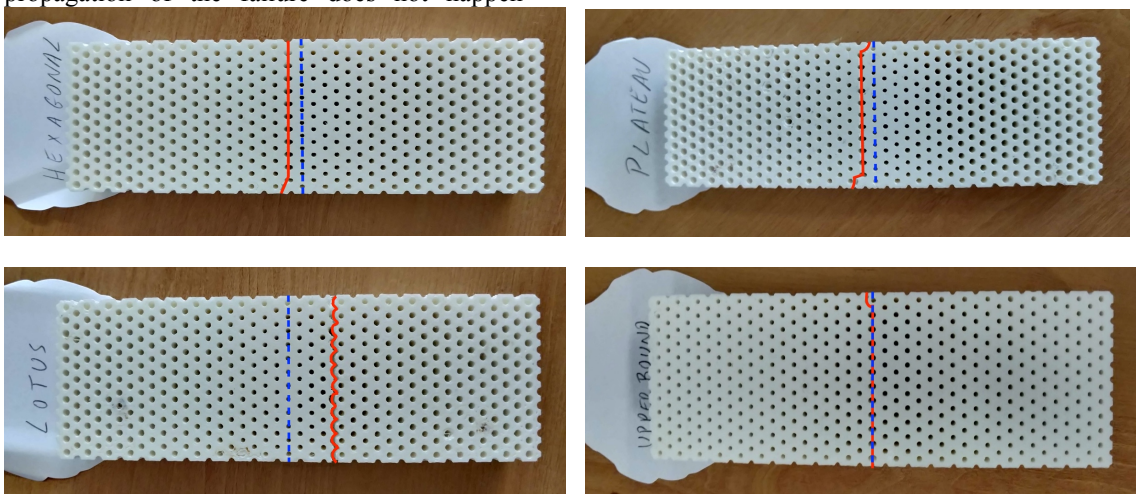

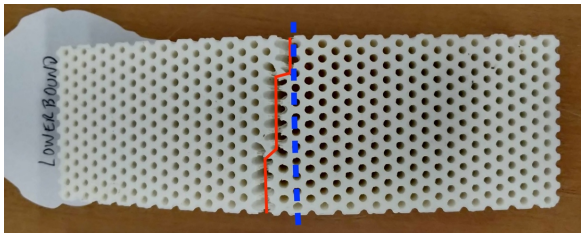


*Figure 13 – Failure mode of the samples, in blue representing the mid-section of the specimen and in red the experimental failure mode.*

## Correlation between methods

Table 10 compare both numerical and experimental results. The numerical results presented in Table 10 are corrected to be for the entire geometry. Analyzing the load-displacement curves of the five structures that were designed to be additively manufactured (Figure 12), it is visible a prevailing of the elastic behavior, although some specimens present a substantial plastic region.

*Table 10 - Comparison between numerical and experimental results, load, K, absorbed energy and von Mises stress.*

| Topology | Load Num (N) | Load Exp (N) | K Num (N/mm) | K Exp (N/mm) | $E_a$ Num (J) | $E_a$ Exp (J) | $\sigma_{(vM)}/\bar{\rho}$ (MPa) |
|---|---|---|---|---|---|---|---|
| **Hexagonal** | 2538.13 | 3466.99 | 1015.25 | 1544.64 | 3.15 | 4.01 | 151.92 |
| **Plateau** | 2553.46 | 3183.08 | 1021.38 | 1375.80 | 3.17 | 3.75 | 155.80 |
| **Lotus** | 2733.37 | 3139.53 | 1093.35 | 1375.61 | 3.40 | 3.69 | 129.30 |
| **Upperbound** | 2517.04 | 2502.49 | 1006.82 | 1098.04 | 3.13 | 2.93 | 147.65 |
| **Lowerbound** | 1814.99 | 1825.76 | 726.00 | 806.22 | 2.26 | 2.12 | 137.52 |

This leads to a more brittle-like fracture, except for the Lowerbound samples that present a ductile fracture. Since the elastic behavior prevails, it justifies performing a linear elastic numerical analysis to compare with the experimental work. For the numerical analysis, the displacement was set to be 2.5 mm and for those values it is clearly visible that all specimens are in the linear region (observable in Figure 12). The numerical results are in agreement with the experimental results. Deviations in the results, (Table 10) may be due to manufacturing defects of the FFF procedure.

# Conclusions

For this thesis, FGCM structures were created using different density gradients, that are characterized by a G parameter. These structures were designed to be applied on sandwich panel cores. The manufacturing of the specimens through FFF allowed the experimental analysis of these structures.

The correspondence between the FEA and the experimental testing was satisfactory, when comparing the loads-displacement results in both methods. For the failure mode, although the FEA showed that the contact area with the moving roller was the area of higher von Mises stress, the failure did not occur in that manner in most cases. That was due to manufacturing defects – Lotus – and due to a slight deviation of the moving roller.

Once the correlation between methods is deemed satisfactory, the FEA results can be validated. For all geometries, the functional graded cellular structures presented a better performance when compared to regular cellular structures in terms of strength, stiffness and absorbed energy.

Geometry wise, in FEA, the geometry with better performance depended on the angle of rotation of the structure. . For 0-degree rotation, structures with G parameter of 0.091, 0.105 and 0.212 Lotus had the better performance. For 90-degree rotation, the structure with highest stiffness was the Hexagonal and the structure with highest absorbed energy value was the Plateau.

When analyzing the Aluminum FEA results, with a G parameter of 0.080 and 0-degree rotation, the geometry with the highest stiffness was the Lotus and the one with highest absorbed energy value was the Plateau.

The core design and the G parameter were found to be the main influences of the

mechanical properties. Having a G parameter influences positively both in stiffness and absorbed energy ability. The structures with G parameter of 0 performed the worst in all parameters. Although the structures with G parameter of 0.212 performed better than the ones with G parameter of 0.091 showing that the performance gets better with the higher G parameter, that was not the case for structures with G parameter of 0.105, which performed slightly worse than structures with G parameter of 0.091.

Finally, this work concludes firstly that the performance of FGCM structures may be better than regular honeycombes, as the former presented both numerically and experimentally higher values of stiffness and energy absorption. Secondly, it may be concluded that the higher the G parameter, the better is the mechanical performance of the structures. Thirdly, for 0-degree rotation, the Lotus structures are superior to the more common Hexagonal ones. Therefore, the FGCM structures may be substitutes to conventional structures in the design of composite panels.

# Bibliography


[1] Ronan, William, et al. "The Tensile Ductility of Cellular Solids: The Role of Imperfections." *International Journal of Solids and Structures*, vol. 102-103, 15 Dec. 2016, pp. 200–213., doi:10.1016/j.ijsolstr.2016.10.004.

[2] Vatanabe, S.l., et al. "Modeling of Functionally Graded Materials." *ComprehensiveMaterials Processing*, 2014, pp. 261–282., doi:10.1016/b978-0-08-096532-1.00222-3.

[3] Miranda, Rosa. "Surface Reinforcements of Light Alloys." *Surface Modification by Solid State Processing*, 2014, pp. 113–152., doi:10.1533/9780857094698.113.

[4] Gibson, Lorna J., and Michael F. Ashby. *Cellular Solids: Structure and Properties*. Cambridge Univ. Press, 2010.

[5] Liang, Minzu, et al. "Theoretical and Numerical Investigation of Blast Responses of Continuous-Density Graded Cellular Materials." *Composite Structures*, vol. 164, Mar. 2017, pp. 170–179., doi: 10.1016/j.compstruct.2016.12.065.

[6] Araújo, Hugo, et al. "The Effect of Geometry on the Flexural Properties of Cellular Core Structures." *Jornal of Materials: Design and Applications*, vol. 233, no. 3, 11 Oct. 2018, pp. 338–347., doi:10.1177/1464420718805511.

[7] Xiao, Lijun, and Weidong Song. "Additively-Manufactured Functionally Graded Ti-6Al-4V Lattice Structures with High Strength under Static and Dynamic Loading: Experiments." *International Journal of Impact Engineering*, vol. 111, 2018, pp. 255–272., doi:10.1016/j.ijimpeng.2017.09.018.

[8] Shady Farah, Daniel G. Anderson, Robert Langer, Physical and mechanical properties of PLA, and their functions in widespread applications — A comprehensive review, Advanced Drug Delivery Reviews, Volume 107, 2016, Pages 367-392, ISSN 0169 409X, https://doi.org/10.1016/j.addr.2016.06.012.

[9] J. Fernandes, A. M. Deus, L. Reis, M. F. Vaz, and M. Leite. "Study of the influence of 3D printing parameters on the mechanical properties of PLA". *Proceedings of the International Conference on Progress in Additive Manufacturing*, May. 2018. ISSN 24248967. doi: 10.25341/D4988C.

[10] Siemens. "siemens nx online guide". in: *Siemens website* (2020). https://docs.plm.automation. siemens.com/tdoc/nx/12/nx_help/#uid:index. Accessed: May-August 2020.

[11] ASTM C393-00. Standard Test Method for Flexural Properties of Sandwich Constructions. Stan- dard, ASTM International, West Conshohocken, PA, Mar. 2000.


# Acknowledgement


The author thanks Professor Maria de Fátima Vaz, Professor Augusto Moita de Deus, Eng. Manuel Sardinha and Frederico Alves.